applied sciences

MDPI

Article

Nonlinear TeraHertz Transmission by Liquid Water at 1 THz

Fabio Novelli [1,*], Chun Yu Ma [1], Nidhi Adhlakha [2], Ellen M. Adams [1], Thorsten Ockelmann [1], Debasish Das Mahanta [1], Paola Di Pietro [2], Andrea Perucchi [2] and Martina Havenith [1,*]

[1] Department of Physical Chemistry II, Ruhr University Bochum, 44801 Bochum, Germany; Chun.Ma@ruhr-uni-bochum.de (C.Y.M.); ellen.adams@ruhr-uni-bochum.de (E.M.A.); thorsten.ockelmann@rub.de (T.O.); Debasish.DasMahanta@rub.de (D.D.M.)

[2] Elettra-Sincrotrone Trieste S.C.p.A, S.S.14 km 163.5, Basovizza, 34149 Trieste, Italy; nidhi.adhlakha@elettra.eu (N.A.); paola.dipietro@elettra.eu (P.D.P.); andrea.perucchi@elettra.eu (A.P.)

* Correspondence: fabio.novelli@ruhr-uni-bochum.de (F.N.); martina.havenith@ruhr-uni-bochum.de (M.H.)

Received: 8 July 2020; Accepted: 27 July 2020; Published: 30 July 2020

check for updates

Abstract: The solvation properties of liquid water originate from the transient network of hydrogen-bonded molecules. In order to probe the coupling between the different modes of this network, nonlinear terahertz (THz) spectroscopy techniques are required. Ideally, these techniques should use a minimal volume and capitalize on sensitive field-resolved detection. Here we performed open aperture z-scan transmission experiments on static liquid cells, and detect the THz fields with electro-optical techniques. We show that it is possible to quantify the nonlinear response of liquid water at ~1 THz even when large signals originate from the sample holder windows.

Keywords: terahertz; nonlinear; water; solvation

1. Introduction

Liquid water strongly absorbs terahertz (THz) radiation [1–9]. Intermolecular interactions determine the unique properties of water [10,11] and can assist biochemical reactions [12,13]. In the low frequency range water displays an overlap of different intermolecular hydrogen bond and Debye-like modes [4,5]. Recent ab initio calculations described infrared (IR) and Raman spectra [14] and separated the intramolecular and intermolecular modes [15]. In order to disentangle the distinct modes, nonlinear techniques are required. This is especially challenging in the THz range due to lack of brilliant sources [4]. To this aim, a variety of nonlinear laser techniques have been used [16–24].

The Hamm group developed a 2D spectroscopic tool that combines two pulses in the visible (Raman excitation) with a THz beam [16,17] and suggested that the intermolecular translational band of water could be characterized by a quasi-inhomogeneous broadening with a correlation time of 370 fs [18]. THz-optical Kerr (TOK) spectroscopy combines an intense THz pump pulse with a weaker optical beam that probes the THz-induced birefringence. In this way, Zalden et al. [19] estimated that the nonlinear molecular alignment of a water dipole can be described with the parameter $B_m^{(2)} = -2.5 \times 10^{-14} \frac{\text{cm}}{\text{V}^2}$, which is on the same order of magnitude of the electronic effect detected by optical-optical Kerr [20,21] experiments (see, e.g., Table 1 in [19]). With TOK, Elgabarty et al. [22,25] recently found indication of a ~0.5 ps long dynamical coupling between rotational and translational intermolecular water modes at low-frequency.

Given the sequence of optical and THz fields, all these nonlinear techniques are sensitive only to modes that are strongly active both in Raman as well as in the far infrared. Thus, a complementary approach is to perform nonlinear experiments employing exclusively THz fields. We previously performed THz-THz Kerr experiments at 12.3 THz with the librational mode of water and found that the THz-induced birefringence is about three orders of magnitude larger than in TOK experiments [24]. Tcypkin et al. [23] reported the nonlinear transmission of almost single-cycle pulses centered at 0.75 THz by a liquid water jet. They performed typical z scan measurements [26], whereby the sample is moved through the beam focus and the intensity transmission is measured with a power detector, both with an open as well as with a partially closed aperture [27,28]. This experimental approach is restricted to the large sample volume required to run a recirculating liquid jet, which to our knowledge needs at least hundreds of milliliters of liquid sample [29]. However, this prevents applications to expensive solutes that are not available in large quantities. In addition, it is preferable to use field-sensitive rather than intensity detectors because of their superior dynamic range [29–31].

In order to overcome these two bottlenecks, here we report nonlinear transmission measurements of ~1 THz pulses by small volumes of liquid enclosed in a static cell with diamond windows. By comparing field- and intensity-resolved z scan experiments, we were able to correctly quantify the nonlinear response of bulk water even in the presence of a large nonlinear signal caused by the empty sample holder.

2. Materials and Methods

We performed experiments at the THz source TeraFERMI [32], located at the free electron laser FERMI at the Elettra synchrotron (Trieste, Italy). The source emitted almost single-cycle pulsed THz fields centered at ~1 THz and at a repetition rate of 50 Hz. The liquid is enclosed in a static cell with 0.5 mm thick diamond windows and a clear aperture of ~25 mm. The pure liquid water thickness is set to ca. 100 or 50 μm with Kapton spacers. The temperature of the sample holder is stabilized to 20 ± 0.05 °C with a recirculating chiller.

The diffusion limited thermalization time of the sample is approximately $t \approx \frac{r^2}{D}$ with D diffusivity and r radius of a sphere of volume equal to the sample volume [33,34]. Considering $D = 1.4 \times 10^{-7} \mathrm{m}^2/\mathrm{s}$ for liquid water and the sample volume, we estimate the thermalization time of the irradiated water to $t \approx 0.3 - 1.7$ s. The repetition rate of the source is 50 Hz (0.02 s), thus up to $15 - 85$ pulses can cumulatively heat up the water sample. Assuming that all the THz power is instantaneously converted into heat, we estimate the temperature increase of the liquid water sample to within $+0.02$ °C and $+0.04$ °C. This temperature increase is lower than the noise level of the recirculating chiller that sets the temperature of the static cell to 20 ± 0.05 °C. For this reason, thermal effects can be disregarded.

The THz radiation is detected with an intensity detector (silicon bolometer) or via field-sensitive electro-optical sampling (EOS). EOS is performed with a 100 μm thick ZnTe crystal. From the optical coefficients [35], the THz spot sizes measured with a camera (Ophir PyrocamIIIHR), and accounting for the reflection losses of the windows, we estimate the maximum THz electric field to be E_0 = 215 kV/cm at the focal position inside the diamond cell.

As sketched in Figure 1, we performed z scan experiments on both the empty as well as the filled cell, and with either intensity (bolometer) or field (EOS) detectors. TeraFERMI is focused with a 4″ diameter off-axis parabolic mirror (OAPM) down to a spot size with full-width at half maximum (FWHM) of ~1.1 mm. The sample position is controlled with a mechanical stage. When the sample holder is placed at the focal position (z = 0), the peak power (P) reaches the largest value P = 100% = 61.4 MW/cm^2. At z = 0, both the empty as well as the water-filled cell display nonlinear transmission (sketched in red in Figure 1a). When the sample is moved away from the focus to z > 22 mm, P decreases below 17% (<10 MW/cm^2, Figure 1b) and approaches the regime of linear transmission. In Figure 1b we show the THz spot size characterized with a THz camera replacing the sample, at the sample position. We note that in this case there is no sample displaying a nonlinear response.

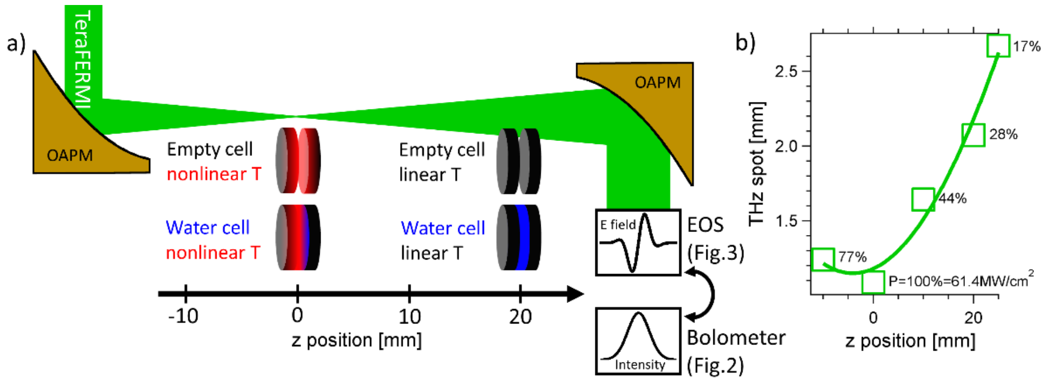

Figure 1. (**a**) Sketch of the experimental setup. The terahertz source is TeraFERMI at the FERMI free-electron laser at the Elettra synchrotron. The beam path of the THz radiation is shown in green and routed with two off-axis parabolic mirror (OAPM). The sample holder is moved through the THz focus with a computer-controlled stage. The nonlinear transmission (red) reaches a maximum at the THz focal position (z = 0). When the static cell is empty, the nonlinear response can originate from the diamond windows (black). When the liquid holder is filled with water (blue), the nonlinear response can also originate from the liquid layer. Away from the focus, the transmission approaches the linear value (z > 20 mm). Two detecting apparatuses are alternatively used to measure the field (electro-optical sampling, EOS) or its intensity (silicon bolometer). (**b**) THz beam properties measured with a camera placed at the sample position. The green squares indicate the full-width at half maximum (FWHM) of the THz spot size measured as a function of the position of the z stage. The solid green line is a guide to the eye. The THz spot is ca. 1.1 mm at the focus z = 0. In this position, the peak power is maximum and amounts to P = 100% = 61.4 MW/cm^2. Moving away from the focus, P decreases for increasing THz spot area.

We characterized previously the optical properties of the diamond windows of the sample holder with linear, tabletop terahertz time-domain spectroscopy (THz-TDS). The details of this linear spectroscopy technique are reported elsewhere [36]. The diamond windows display a small absorption in the THz range (orange diamonds, Figure 2a). The frequency-dependent absorption coefficient $\alpha(\omega)$ can be fitted to [37] the Drude model as shown in Figure 2b and Equation (1):

$$\alpha(\omega) = \frac{eN_c\gamma^2\mu}{\varepsilon_0 nc(\omega^2+\gamma^2)} \tag{1}$$

where e is the electric charge, N_c is the concentration of free charge carriers, γ is the scattering rate, μ is the carriers mobility, ε_0 is the free space permittivity, n is the index of refraction, and c is the speed of light. From the fit we estimate $N_c \approx 1.13 \times 10^{-14} \mathrm{cm}^{-3}$, which corresponds to ca. 6 free carriers in 10 billion carbon atoms of a diamond window. Even for such low carrier doping the THz transmission of a crystal can display a nonlinear response, and the THz absorption can drop by 80% [37].

3. Results and Discussion

In Figure 2c we show open aperture z scan measurements, where the bolometer detects the THz intensity (I) transmitted by the empty (I_0, black in Figure 2c) and water-filled cell (I_{wat}, blue in Figure 2c). In order to compare the different transmission values of filled and empty cell, the intensity is in each case normalized to the corresponding value of the transmission at low peak power, I(z = 22 mm). The absolute value of the transmission by the filled cell is different than the transmission by the empty cell, because liquid water strongly absorbs THz radiation [33]. Thus, we plot the relative transmission values in Figure 2c: $\frac{I_0(z)}{I_0(z=22\ \mathrm{mm})}$ for the empty cell, and $\frac{I_{wat}(z)}{I_{wat}(z=22\ \mathrm{mm})}$ for the water-filled static sample holder. The transmission at $z = 22$ mm is the furthest point from the focus given the range of the mechanical stage, the peak power is reduced to the lowest possible value of ca. 10 MW/cm^2, and the transmission approaches the linear regime. Given the restricted beam time available, we were not able to acquire more data while keeping the same signal-to-noise. For this reason, the z scan measurements in, e.g., Figure 2c display a limited number of discrete points.

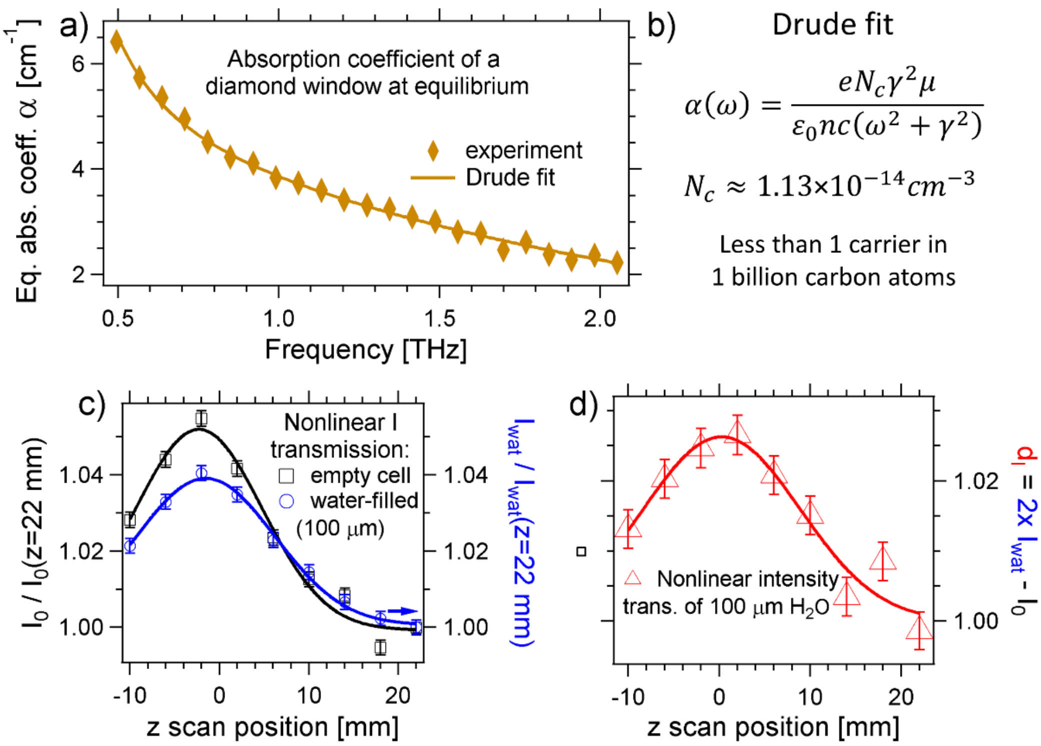

Figure 2. (**a**) Absorption coefficient of a single diamond window of the empty sample holder measured with linear THz time-domain spectroscopy. (**b**) The absorption can be fitted to a Drude peak with few free carriers, corresponding to less than one carrier per billion carbons. (**c**) Z scan measurements of the THz intensity transmitted by the empty diamond cell (black), and of the liquid cell filled with a 100-micron thick water layer (blue). The error bars are the standard error of the mean calculated from 300 measurements. The squares and circles are the experimental results, the solid lines are guides to the eye. (**d**) The nonlinear intensity transmission of the water layer is estimated as the difference of the intensity transmissions of filled and empty cell (d_I). The solid red line is a Gaussian fit. The experiments reported in Panels c–d are performed with an intensity detector (bolometer).

As shown in Figure 2c, and expected for nonlinear transmission, the detected THz intensity varies as a function of the position of the z stage and is maximum around the focal point (z = 0). If the nonlinear response would be restricted to the diamond windows, we expect for the empty cell the nonlinear response of the two windows. In case of the water-filled cell, the THz intensity at the second diamond window is decreased by ca. 90% [33], therefore, the THz nonlinear response by the second diamond window can be neglected only when the liquid cell is filled. If water would not contribute to the nonlinearity, then the nonlinear response by the filled cell should be approximately half of the nonlinear response of the empty cell (one vs. two windows). However, by inspecting Figure 2c we note that the transmission of the water-filled cell increases by ca. 4% ($\frac{I_{wat}(z=0)}{I_{wat}(z=22\text{ mm})} \sim 1.04$), while the transmission by the empty sample holder increases by ~5% ($\frac{I_0(z=0)}{I_0(z=22\text{ mm})} \sim 1.05$). This suggests that both the front diamond window as well as liquid water display nonlinear transmission when the cell is filled. In order to estimate the nonlinear THz intensity transmission by water (Equation (2)), we plot

$$d_I(z) = 2 \times \frac{I_{wat}(z)}{I_{wat}(z = 22\text{ mm})} - \frac{I_0(z)}{I_0(z = 22\text{ mm})} \quad (2)$$

in Figure 2d. The factor two, roughly accounts for the fact that two diamond windows contribute to the nonlinear transmission of the empty sample holder, while only one diamond window contributes to the water-filled cell nonlinear transmission. The amplitude of d_I at the THz focus can be estimated to 1.026 ± 0.008 with a Gaussian function (solid red line in Figure 2d).

When the electromagnetic power (P) increases up to the nonlinear response regime, the absorption coefficient of a material can be written as Equation (3) [27]:

$$\alpha(\mathrm{P}) = \alpha + \alpha^{\mathrm{NL}} \times \mathrm{P}, \tag{3}$$

where α is the linear absorption term, and α^{NL} quantifies the nonlinear contribution that increases with P. When the sign of α^{NL} is negative, the absorption decreases and the nonlinear response can be described as saturable absorption or bleaching. Open aperture z scan intensity measurements are insensitive to the nonlinear refraction [26], and can quantify the nonlinear absorption term (Equation (4)) as in [27]:

$$\alpha^{\mathrm{NL}} \approx (1 - \mathrm{d_I}(0)) \frac{\alpha}{\mathrm{P} \times (1 - e^{-\alpha \mathrm{L}})}, \tag{4}$$

where L is the sample thickness. From the value $\mathrm{d_I}(0)$ = 1.026 ± 0.008 obtained from Figure 2d, the THz peak power P = 61.4 MW/cm^2, the sample thickness, and the equilibrium absorption coefficient of water [33] (α = 197.4 cm^{-1} at 1 THz), we obtain $\alpha^{\mathrm{NL}}_{\mathrm{wat}} = -87 \pm 27\ \mathrm{cm/GW}$. Within the error bars, this value agrees with $\alpha^{\mathrm{NL}}_{\mathrm{wat}} \approx -78\ \mathrm{cm/GW}$ estimated from Figure 2a of [23]. To achieve the first approximation, in the data analysis we assumed that the nonlinear transmissions of both the two diamond windows of the empty cell, as well as of the empty and filled cell, are additive. Following these assumptions, we estimated a nonlinear absorption for liquid water that agrees with previous results. This good agreement confirms the validity of the approximations used.

In the next step, we want to investigate the nonlinear response of the index of refraction (Equation (5)). In the simplest case:

$$\mathrm{n}(\mathrm{P}) = \mathrm{n} + \mathrm{n}^{\mathrm{NL}} \times \mathrm{P}, \tag{5}$$

where n is the linear refraction term, and n^{NL} (also called n_2 or Kerr term) quantifies the nonlinear contribution. Open aperture z scan measurements performed with an intensity detector (e.g., bolometer, Figure 2), are sensitive to absorption variations, but not to n^{NL}. The nonlinear refractive index is typically measured by comparing open and partially closed aperture z scan experiments, both measured with an intensity detector. Here we suggest that a field-sensitive detector should be able to probe simultaneously both the changes in the extinction coefficient as well as in the index of refraction, possibly with better resolution. In order to prove this assumption, we performed additional open aperture z scan measurements on the empty and the water-filled diamond cell, and detected the transmitted THz peak field with EOS. Time resolved THz experiments or "pump scans" are routinely performed at the peak position of the THz field, and allow estimating the overall size of the signal and the dynamics [38]. Contrarily to intensity measurements with, e.g., a bolometer, the amplitude of the THz peak is affected not only by the change in absorption, but also by the change of the index of refraction of the sample, which can delay the pulse in time [38]. For this reason, by comparing the results of z scan measurements performed with bolometer and field-sensitive techniques, in the following we estimate the nonlinear absorption and the nonlinear refraction.

In Figure 3a we show the full THz fields transmitted by the empty cell (black) and by the diamond cell filled with a 50 µm thick water layer (blue). The peak THz field transmitted by the water-filled (empty) sample holder is marked with $\mathrm{E_{wat}}$ ($\mathrm{E_0}$). In Figure 3b we show open aperture z scan measurements, where the balanced EOS detection measures the peak amplitude of the THz field (E) transmitted by the empty ($\mathrm{E_0}$, black in Figure 3b) and water-filled cell ($\mathrm{E_{wat}}$, blue in Figure 3b).

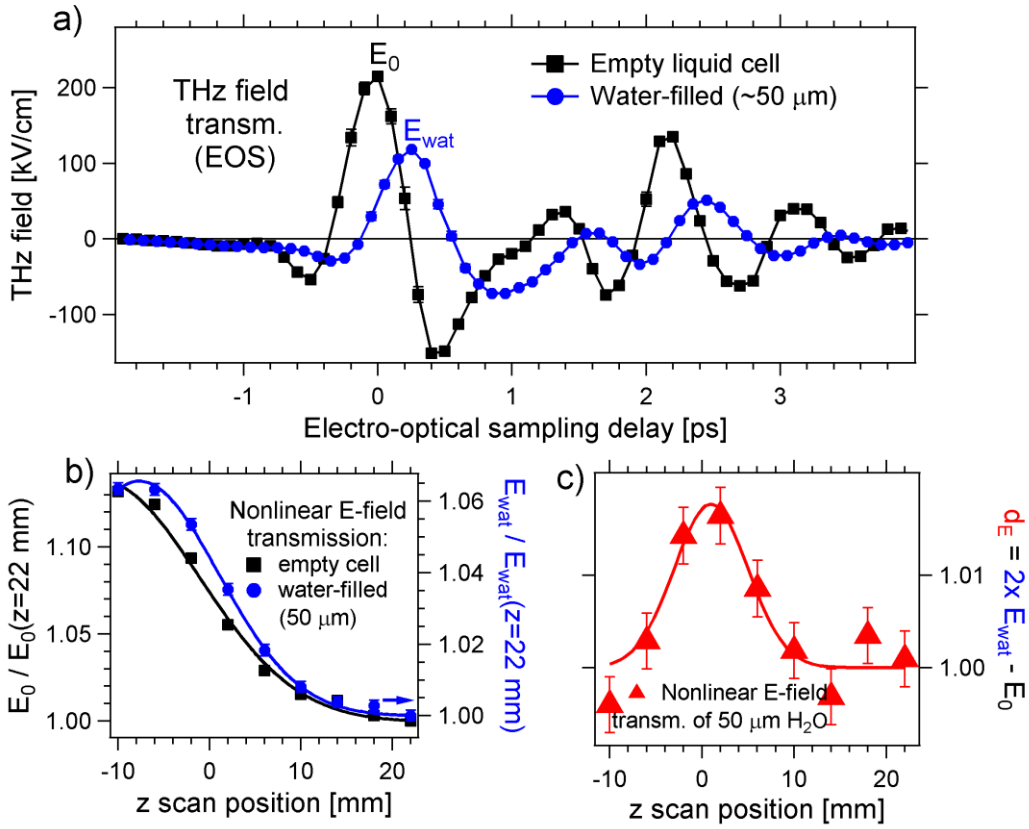

Figure 3. (**a**) We used a 100 μm ZnTe crystal to detect the THz field transmitted by the empty cell holder (black), and by the sample holder filled with a 50-micron thick layer of pure water (blue). The peak THz field transmitted by the empty (water-filled) cell is marked with E_0 (E_{wat}). (**b**) Z scan measurements of the peak field transmission of the empty diamond cell (black), and of the liquid cell filled with a 50-micron thick water layer (blue). The error bars are indicated and correspond to the standard error of the mean calculated from 100 measurements. Solid circles and squares represent the experimental results. Solid lines are guides to the eye. (**c**) The nonlinear field transmission of the water layer is estimated to the difference of the field transmissions of filled and empty cells (d_E). The red solid line is a Gaussian fit. The experiments in Panels b–c are performed with a field detector (EOS).

In order to compare the electric field transmitted by the filled and empty cell, the field is in each case normalized to the value of the transmission at low THz power, E(z = 22 mm). As shown in Figure 3b and expected for nonlinear transmission, the detected THz peak field varies as a function of the position of the z stage. However, in these field-sensitive experiments the maximum signal is not found at z = 0. This originates from a small drift of the THz spot size imaged at the detection crystal, which was checked with the THz camera and is unchanged for empty and filled cell. This systematic error can be present only when detecting the field amplitude and not the area-integrated signal (e.g., bolometer, Figure 2). This can be removed by comparing the two z scan experiments. In order to quantify the nonlinear field transmission by the water layer (Equation (6)), we use the same approach outlined above for the intensity transmission (Figure 2d). The quantity:

$$d_E(z) = 2 \times \frac{E_{wat}(z)}{E_{wat}(z = 22\ \mathrm{mm})} - \frac{E_0(z)}{E_0(z = 22\ \mathrm{mm})} \tag{6}$$

is shown in Figure 3c. The amplitude of d_E at the THz focus can be estimated to 1.018 ± 0.005 with a Gaussian function (solid red line in Figure 3c). We chose a slightly different spacer for EOS z scans (50 μm, Figure 3) with respect to the intensity measurements (100 μm, Figure 2). As expected, for the thinner spacer the THz response is "sharper": the nonlinear water signal is evident over a narrower range around z = 0 when the thinner spacer is used (compare Figure 3c with Figure 2d).

Routine z scan measurements are obtained either with an open or a partially closed aperture in front of the detector [23]. Often, z scan experiments measure only the transmitted intensity with, e.g., a bolometer or a diode, and not the field transmittance [26–28]. An open aperture intensity z scan allows to quantify only the nonlinear absorption (α^{NL}) [26], while a partially closed aperture intensity z scan is sensitive both to the nonlinear absorption as well as the nonlinear refraction [26]. The nonlinear refractive index (n^{NL}) can be estimated by comparing two intensity-sensitive z scans, obtained either with open or partially closed aperture [26]. Here we propose to replace the closed aperture intensity z scan, with an open aperture field z scan. The transmitted field measured with, e.g., EOS detection, must depend on the nonlinear absorption and, through the change of the spot size induced by the Kerr lensing, also on the nonlinear refraction. The advantage of field-sensitive z scan is the superior dynamic range, which can exceed 60 dbm as we demonstrated recently for THz-TDS based on an amplified laser [29].

The nonlinear refractive index can be estimated as shown in Equation (7) [23]:

$$n^{NL} = \Delta T \frac{\alpha}{P \times (1 - e^{-\alpha L})} \frac{\lambda}{1.8 \times (1 - S)^{0.25}}, \tag{7}$$

where ΔT is the modulation of a z scan estimated as the difference between minimum and maximum transmission, λ is the radiation wavelength, and S is the linear transmission of the aperture. This equation is strictly valid only when comparing intensity-resolved z scan experiments with different apertures, but we use it in the following to estimate tentatively the nonlinear refraction by comparing intensity- and field-resolved measurements. To first approximation we assume $S = 0$. For simplicity, we assume that the refraction-induced transmission change ΔT (Equation (8)) corresponds to the difference between the nonlinear transmission detected with a field detector (which depends on both α^{NL} as well as n^{NL} [38]) and the nonlinear transmission acquired with an intensity detector (which depends only on α^{NL} [27]):

$$\Delta T \approx (d_E(0))^2 - d_I(0) - 1 = 0.0094 \pm 0.0038, \tag{8}$$

where the first term is squared to account for the relation between field and intensity. Thus, the nonlinear refraction of pure liquid water at ~1 THz corresponds to $n^{NL}_{wat} = (6.5 \pm 2.6) \times 10^{-10} cm^2/W$. Within the error bars, this value agrees again with the value $n^{NL}_{wat} \approx 7 \times 10^{-10} cm^2/W$ reported by Tcypkin et al. [23] for a water jet. This additional benchmark confirms that while some of the above approximations are crude, they provide correct estimation of the magnitude of both amplitude as well as phase nonlinearities displayed by liquid water at ~1 THz.

In the data analysis we neglected the contribution of multiple reflections coming from the cell windows. We note that when we measured the THz peak field (Figure 3), the reflections originating from the layer between the diamond windows are delayed. This can be estimated to twice the layer thickness divided by the speed of light, resulting in a delay of ca. 0.5 ps. As the near-infrared pulse used for the electro-optical sampling detection is shorter than 0.1 ps [32], the ~0.5 ps delay moves the reflected field outside the detection window. However, when we measured the THz intensity with a power detector (Figure 2), the THz beams originating from multiple reflections are fully detected. The most intense THz pulse, with intensity P_0, is the one transmitted at every interface. The first and most intense reflected beam originates from two reflections at the air-diamond interface when the empty cell is measured. We estimate the intensity of the first reflection with Fresnel coefficients as:

$$P_1 \approx \left[\left(\frac{n_{dia} - n_{air}}{n_{dia} + n_{air}} \right) \times \left(\frac{n_{dia} - n_{air}}{n_{dia} + n_{air}} \right) \right]^2 \times P_0 \approx 7 \times 10^{-3} \times P_0 \tag{9}$$

where $n_{dia} \approx 1.8$ ($n_{air} \approx 1$) is the index of refraction of the diamond window (air) at ca. 1 THz, and the second power accounts for the relation between field amplitude and intensity. The intensity of the second reflected beam, which originates from four reflections at the air-diamond interface, is even smaller ($P_2 \approx 4 \times 10^{-5} \times P_0$). Equation (9) indicates that by neglecting the first multiple reflection we induce a systematic error of less than 1%. We previously estimated the nonlinear absorption of liquid water to $\alpha_{wat}^{NL} = -87 \pm 27$ cm/GW and the nonlinear refraction to $n_{wat}^{NL} = (6.5 \pm 2.6) \times 10^{-10} cm^2/W$. Both terms have statistical errors within 30% and 40%. Thus, we can neglect the < 1% systematic error induced by the multiple reflections. Finally, we note that when the cell is filled, liquid water strongly absorbs THz radiation [33] and the effect of multiple reflections is further reduced.

The ab initio molecular dynamics (MD) calculations with static (DC) fields by Cassone et al. [14] suggest that the absorption at ~1 THz by liquid water should decrease for increasing DC field strengths. This could be consistent with the experimental observation that the nonlinear absorption coefficient of water is negative ($\alpha_{wat}^{NL} = -87 \pm 27$ cm/GW), i.e., water is more transparent and absorbs less radiation for increasing field strength. However, it is important to note that the THz source used here is not DC [39,40], but emits almost single-cycle pulses centered at ~1 THz. New experiments and theory are needed to clarify the origin of both the absorptive (α_{wat}^{NL}) as well as the refractive (n_{wat}^{NL}) nonlinearities detected here in bulk liquid water. We speculate that these large anisotropies might stem from the local asymmetry in the strength of the hydrogen bonds [25] and/or be rooted in the resonant enhancement of molecular reorientations [24].

In conclusion, we have shown that the full nonlinear THz transmission properties of liquid water can be deduced from measurements performed in a static cell with windows. Field-resolved detection allows estimation of both the real as well as the imaginary nonlinear optical coefficients, even when only open aperture z-scan transmission measurements are performed. Given the small sample volume required, this technique can be readily applied to assess the transient solvation dynamics even of complex solutes in aqueous environments, and could be useful to other research fields. Extensions of this novel experimental approach could also help to clarify the recent, puzzling, and mounting evidence of temporally delayed THz responses by liquid water [24,41–43].

Author Contributions: Conceptualization, F.N.; methodology, F.N. and E.M.A.; software, N.A., P.D.P., A.P.; validation, F.N., C.Y.M., N.A., T.O., D.D.M., P.D.P., A.P.; formal analysis, F.N.; investigation, F.N., C.Y.M., N.A., E.M.A., T.O., D.D.M., P.D.P., A.P.; resources, all authors; data curation, all authors; writing—original draft preparation, F.N., E.M.A., P.D.P., A.P., and M.H.; writing—review and editing, F.N. and E.M.A.; visualization, F.N.; supervision, F.N., A.P., and M.H.; project administration, F.N., A.P., and M.H.; funding acquisition, M.H. All authors have read and agreed to the published version of the manuscript.

Funding: M.H. acknowledges funding by the ERC Advanced Grant 695437. Funded by the Deutsche Forschungsgemeinschaft (DFG, German Research Foundation) under Germany's Excellence Strategy–EXC 2033–390677874–RESOLV.

Acknowledgments: We are grateful to K. Aoki for experimental support.

Conflicts of Interest: The authors declare no conflicts of interest.

References

1. Zelsmann, H.R. Temperature dependence of the optical constants for liquid H2O and D2O in the far IR region. *J. Mol. Struct.* **1995**, *350*, 95–114. [CrossRef]
2. Bertie, J.E.; Lan, Z. Infrared Intensities of Liquids XX: The Intensity of the OH Stretching Band of Liquid Water Revisited, and the Best Current Values of the Optical Constants of H 2 O(l) at 25 °C between 15,000 and 1 cm^{-1}. *Appl. Spectrosc.* **1996**, *50*, 1047–1057. [CrossRef]
3. Ellison, W.J. Permittivity of Pure Water, at Standard Atmospheric Pressure, over the Frequency Range 0–25 THz and the Temperature Range 0–100 °C. *J. Phys. Chem. Ref. Data* **2007**, *36*, 1–18. [CrossRef]
4. Novelli, F.; Guchhait, B.; Havenith, M. Towards Intense THz Spectroscopy on Water: Characterization of Optical Rectification by GaP, OH1, and DSTMS at OPA Wavelengths. *Materials* **2020**, *13*, 1311. [CrossRef]

5. Heyden, M.; Sun, J.; Funkner, S.; Mathias, G.; Forbert, H.; Havenith, M.; Marx, D. Dissecting the THz spectrum of liquid water from first principles via correlations in time and space. *Proc. Natl. Acad. Sci. USA* **2010**, *107*, 12068–12073. [CrossRef]
6. Novelli, F.; Bernal Lopez, M.; Schwaab, G.; Roldan Cuenya, B.; Havenith, M. Water Solvation of Charged and Neutral Gold Nanoparticles. *J. Phys. Chem. B* **2019**, *123*, 6521–6528. [CrossRef]
7. Alfarano, S.R.; Vondracek, H.; Sebastiani, F.; Novelli, F.; Hoberg, C.; Kolling, I.; Brubach, J.-B.; Roy, P.; Schwaab, G.; Havenith, M.; et al. Does hydrated glycine act as solidification nucleus at multi-kilobar conditions? *Biophys. Chem.* **2019**, *253*, 106215. [CrossRef]
8. Vondracek, H.; Alfarano, S.; Hoberg, C.; Kolling, I.; Novelli, F.; Sebastiani, F.; Brubach, J.-B.; Roy, P.; Schwaab, G.; Havenith, M.; et al. Urea's match in the hydrogen-bond network? A high pressure THz study. *Biophys. Chem.* **2019**, *254*, 106240. [CrossRef]
9. Bergonzi, I.; Mercury, L.; Brubach, J.-B.; Roy, P. Gibbs free energy of liquid water derived from infrared measurements. *Phys. Chem. Chem. Phys.* **2014**, *16*, 24830–24840. [CrossRef]
10. Ball, P. Water — an enduring mystery. *Nature* **2008**, *452*, 291–292. [CrossRef]
11. Nilsson, A.; Pettersson, L.G.M. The structural origin of anomalous properties of liquid water. *Nat. Commun.* **2015**, *6*, 8998. [CrossRef] [PubMed]
12. Mukherjee, A.; Lavery, R.; Bagchi, B.; Hynes, J.T. On the molecular mechanism of drug intercalation into DNA: A simulation study of the intercalation pathway, free energy, and DNA structural changes. *J. Am. Chem. Soc.* **2008**, *130*, 9747–9755. [CrossRef] [PubMed]
13. Wilhelm, M.; Mukherjee, A.; Bouvier, B.; Zakrzewska, K.; Hynes, J.T.; Lavery, R. Multistep drug intercalation: Molecular dynamics and free energy studies of the binding of daunomycin to DNA. *J. Am. Chem. Soc.* **2012**, *134*, 8588–8596. [CrossRef] [PubMed]
14. Cassone, G.; Sponer, J.; Trusso, S.; Saija, F. Ab initio spectroscopy of water under electric fields. *Phys. Chem. Chem. Phys.* **2019**, *21*, 21205–21212. [CrossRef] [PubMed]
15. Sommers, G.M.; Calegari Andrade, M.F.; Zhang, L.; Wang, H.; Car, R. Raman spectrum and polarizability of liquid water from deep neural networks. *Phys. Chem. Chem. Phys.* **2020**, *22*, 10592–10602. [CrossRef]
16. Savolainen, J.; Ahmed, S.; Hamm, P. Two-dimensional Raman-terahertz spectroscopy of water. *Proc. Natl. Acad. Sci. USA* **2013**, *110*, 20402–20407. [CrossRef]
17. Shalit, A.; Ahmed, S.; Savolainen, J.; Hamm, P. Terahertz echoes reveal the inhomogeneity of aqueous salt solutions. *Nat. Chem.* **2017**, *9*, 273–278. [CrossRef]
18. Sidler, D.; Hamm, P. Feynman diagram description of 2D-Raman-THz spectroscopy applied to water. *J. Chem. Phys.* **2019**, *150*, 044202. [CrossRef]
19. Zalden, P.; Song, L.; Wu, X.; Huang, H.; Ahr, F.; Mücke, O.D.; Reichert, J.; Thorwart, M.; Mishra, P.K.; Welsch, R.; et al. Molecular polarizability anisotropy of liquid water revealed by terahertz-induced transient orientation. *Nat. Commun.* **2018**, *9*, 2142. [CrossRef]
20. Taschin, A.; Bartolini, P.; Eramo, R.; Righini, R.; Torre, R. Evidence of two distinct local structures of water from ambient to supercooled conditions. *Nat. Commun.* **2013**, *4*, 2401. [CrossRef]
21. Taschin, A.; Bartolini, P.; Fanetti, S.; Lapini, A.; Citroni, M.; Righini, R.; Bini, R.; Torre, R. Pressure Effects on Water Dynamics by Time-Resolved Optical Kerr Effect. *J. Phys. Chem. Lett.* **2020**, *11*, 3063–3068. [CrossRef] [PubMed]
22. Elgabarty, H.; Kampfrath, T.; Bonthuis, D.J.; Balos, V.; Kaliannan, N.K.; Loche, P.; Netz, R.R.; Wolf, M.; Kühne, T.D.; Sajadi, M. Energy transfer within the hydrogen bonding network of water following resonant terahertz excitation. *Sci. Adv.* **2020**, *6*, eaay7074. [CrossRef] [PubMed]
23. Tcypkin, A.N.; Melnik, M.V.; Zhukova, M.O.; Vorontsova, I.O.; Putilin, S.E.; Kozlov, S.A.; Zhang, X.-C. High Kerr nonlinearity of water in THz spectral range. *Opt. Express* **2019**, *27*, 10419. [CrossRef] [PubMed]
24. Novelli, F.; Ruiz Pestana, L.; Bennett, K.C.; Sebastiani, F.; Adams, E.M.; Stavrias, N.; Ockelmann, T.; Colchero, A.; Hoberg, C.; Schwaab, G.; et al. Strong Anisotropy in Liquid Water upon Librational Excitation Using Terahertz Laser Fields. *J. Phys. Chem. B* **2020**, *124*, 4989–5001. [CrossRef] [PubMed]
25. Elgabarty, H.; Kühne, T.D. Tumbling with a limp: Local asymmetry in water's hydrogen bond network and its consequences. *Phys. Chem. Chem. Phys.* **2020**, *22*, 10397–10411. [CrossRef]
26. Sheik-Bahae, M.; Said, A.A.; Wei, T.-H.; Hagan, D.J.; Van Stryland, E.W. Sensitive measurement of optical nonlinearities using a single beam. *IEEE J. Quantum Electron.* **1990**, *26*, 760–769. [CrossRef]

27. Zheng, X.; Chen, R.; Shi, G.; Zhang, J.; Xu, Z.; Cheng, X.; Jiang, T. Characterization of nonlinear properties of black phosphorus nanoplatelets with femtosecond pulsed Z-scan measurements. *Opt. Lett.* **2015**, *40*, 3480. [CrossRef]
28. Melnik, M.; Vorontsova, I.; Putilin, S.; Tcypkin, A.; Kozlov, S. Methodical inaccuracy of the Z-scan method for few-cycle terahertz pulses. *Sci. Rep.* **2019**, *9*, 9146. [CrossRef]
29. Hoberg, C.; Balzerowski, P.; Havenith, M. Integration of a rapid scanning technique into THz time-domain spectrometers for nonlinear THz spectroscopy measurements. *AIP Adv.* **2019**, *9*, 035348. [CrossRef]
30. Pupeza, I.; Huber, M.; Trubetskov, M.; Schweinberger, W.; Hussain, S.A.; Hofer, C.; Fritsch, K.; Poetzlberger, M.; Vamos, L.; Fill, E.; et al. Field-resolved infrared spectroscopy of biological systems. *Nature* **2020**, *577*, 52–59. [CrossRef]
31. Novelli, F.; Ostovar Pour, S.; Tollerud, J.; Roozbeh, A.; Appadoo, D.R.T.T.; Blanch, E.W.; Davis, J.A. Time-Domain THz Spectroscopy Reveals Coupled Protein–Hydration Dielectric Response in Solutions of Native and Fibrils of Human Lysozyme. *J. Phys. Chem. B* **2017**, *121*, 4810–4816. [CrossRef] [PubMed]
32. Adhlakha, N.; Di Pietro, P.; Piccirilli, F.; Cinquegrana, P.; Di Mitri, S.; Sigalotti, P.; Spampinati, S.; Veronese, M.; Lupi, S.; Perucchi, A. The TeraFERMI Electro-Optic Sampling Set-Up for Fluence-Dependent Spectroscopic Measurements. *Condens. Matter* **2020**, *5*, 8. [CrossRef]
33. Novelli, F.; Chon, J.W.M.; Davis, J.A. Terahertz thermometry of gold nanospheres in water. *Opt. Lett.* **2016**, *41*, 5801. [CrossRef] [PubMed]
34. Luong, T.Q.; Xu, Y.; Bründermann, E.; Leitner, D.M.; Havenith, M. Hydrophobic collapse induces changes in the collective protein and hydration low frequency modes. *Chem. Phys. Lett.* **2016**, *651*, 1–7. [CrossRef]
35. Casalbuoni, S.; Schlarb, H.; Schmidt, B.; Schmüser, P.; Steffen, B.; Winter, A. Numerical studies on the electro-optic detection of femtosecond electron bunches. *Phys. Rev. Spec. Top.-Accel. Beams* **2008**, *11*, 072802. [CrossRef]
36. Adams, E.M.; Lampret, O.; König, B.; Happe, T.; Havenith, M. Solvent dynamics play a decisive role in the complex formation of biologically relevant redox proteins. *Phys. Chem. Chem. Phys.* **2020**, *22*, 7451–7459. [CrossRef]
37. Hebling, J.; Hoffmann, M.C.; Hwang, H.Y.; Yeh, K.-L.; Nelson, K.A. Observation of nonequilibrium carrier distribution in Ge, Si, and GaAs by terahertz pump–terahertz probe measurements. *Phys. Rev. B* **2010**, *81*, 035201. [CrossRef]
38. Beard, M.C.; Turner, G.M.; Schmuttenmaer, C.A. Terahertz Spectroscopy. *J. Phys. Chem. B* **2002**, *106*, 7146–7159. [CrossRef]
39. Shafiei, M.; von Domaros, M.; Bratko, D.; Luzar, A. Anisotropic structure and dynamics of water under static electric fields. *J. Chem. Phys.* **2019**, *150*, 074505. [CrossRef]
40. Shafiei, M.; Ojaghlou, N.; Zamfir, S.G.; Bratko, D.; Luzar, A. Modulation of structure and dynamics of water under alternating electric field and the role of hydrogen bonding. *Mol. Phys.* **2019**, *117*, 3282–3296. [CrossRef]
41. Huang, H.H.; Nagashima, T.; Yonezawa, T.; Matsuo, Y.; Ng, S.H.; Juodkazis, S.; Hatanaka, K. Giant enhancement of THz wave emission under double-pulse excitation of thin water flow. *Appl. Sci.* **2020**, *10*, 2031. [CrossRef]
42. Yiwen, E.; Jin, Q.; Zhang, X.C. Enhancement of terahertz emission by a preformed plasma in liquid water. *Appl. Phys. Lett.* **2019**, *115*, 1–5.
43. Tsubouchi, M.; Hoshina, H.; Nagai, M.; Isoyama, G. Plane photoacoustic wave generation in liquid water using irradiation of terahertz pulses. *arXiv* **2019**, arXiv:1911.04674.